DOI: 10.1002/ejic.201000715

(Carboxymethyl–Dextran)-Modified Magnetic Nanoparticles Conjugated to Octreotide for MRI Applications

Guo-Cheng Han,[a,b] Yang Ouyang,[c] Xue-Ying Long,[c] Yu Zhou,[a] Meng Li,[a] You-Nian Liu,*[a] and Heinz-Bernhard Kraatz*[b]

Keywords: Bioconjugates / Octreotide / Endocytosis / Magnetic resonance imaging

The synthesis of (octreotide–carboxymethyl–dextran)-modified magnetic nanoparticles (CMD-MNPs), which were characterized by FT-IR, AFM, TEM and XRD, and magnetic hysteresis, is described. Magnetic Resonance Imaging (MRI) experiments were performed on a 1.5 Tesla Magnetom Vision machine. The internalization of CMD-MNPs-OC into pancreatic cancer cells Bx-PC3 and colon cancer cells HCT-116 were investigated by transmission electron microscopy (TEM) and magnetic resonance imaging (MRI). The nanoparticles can be recognized specifically, via the somatostatin receptor, and which can be used as a T_2 MRI contrast agent. TEM and MRI results show that somatostatin receptor can deliver OC-modified MNPs into the cytoplasm of a cancer cell line.

Introduction

Over the years, magnetic resonance imaging (MRI) has quickly developed into a powerful diagnostic method that provides reasonable contrast and spatial resolution.[1] It is now routinely used to study the hemodynamic response of the human brain and the spinal cord.[2] The contrast can be enhanced with the help of paramagnetic additives. In recent years, magnetic nanoparticles (NPs) have been explored for biomedical applications including as magnetic carriers for drug delivery systems and contrast enhancement agents.[3] In addition, magnetic NPs display interesting properties including super-paramagnetic characteristics and higher saturation magnetization which are beneficial for imaging, and, in general, they exhibit good biocompatibility.[4–6] However, their use has been hampered not only by issues related to the scale up of the NP synthesis,[7] but there are also issue related to their modification. In particular polymer modifications show promise in drug delivery and for MRI applications, reduce the risk of aggregation and enhance the half-life in vivo.[8,9] Aggregation of NPs will result in the loss of magnetic characteristics, decrease of surface activity, and rapid elimination by macrophages or the reticular endothelial system (RES) before they actually arrive at the target cells. These drawbacks prevent effective loading of drugs or cell-labeling molecules.[10] NPs encapsulation by a polymer shell is an effective way to overcome some of these problems,[11] and additionally enhances their biocompatibility, drug-loading and controlled release, and offers a potential for targeted delivery.[12] Dextran, a biodegradable polysaccharide that is poly-cationic, hydrophilic and containing poly-hydroxy groups that has been explored for coating of magnetic NPs.[13] Particle size and reduction of the terminal glucose of dextran appear to yield more stable NPs.[14] It is important to recognize that the dextran modification of NPs offers the possibility for further modification of the conjugate. Peptide modifications in particular are of importance as they potentially allow to direct the NPs to a specific target.

The neuropeptide somatostatin is a cyclic peptide comprised of 14 amino acids originally isolated from bovine hypothalamus and identified as a potent inhibitor of GH secretion. This peptide exerts a wide variety of inhibitory effects on the endocrine, exocrine, and neural function, and plays an important role in the secretion of hormones, such as insulin, glucagon and the growth hormone.[15,16] Pituitary adenomas and several neuroendocrine tumours such as pancreas and lung cancer over-express somatostatin receptors.[17] In this study, we decided to work with octrotide (OC), which is a synthetic somatostatin analogue that specifically targets somatostatin receptors. OC was developed for the suppression of somatostatin hypersecretion to control neuroendocrine disease symptoms.[18,19] It contains eight amino acids retaining an internal disulfide crosslink (Cys-Cys) to constrain the geometry of the four essential amino acids (Phe3, Trp4, Lys5, Thr6) (see Figure S1, Supporting Information). Clinical studies have shown that OC has a significantly longer therapeutic half-life compared to soma-

[a] College of Chemistry and Chemical Engineering, Central South University,
Changsha, Hunan 410083, P. R. China
Fax: +86-731-8883-6964
E-mail: liuyoun@mail.csu.edu.cn
[b] Department of Chemistry, the University of Western Ontario, London, Ontario N6A 5B7, Canada
Fax: +1-519-661-3022
E-mail: hkraatz@uwo.ca
[c] Xiangya Hospital, Central South University, Changsha, Hunan 410078, P. R. China

Supporting information for this article is available on the WWW under http://dx.doi.org/10.1002/ejic.201000715.

 © 2010 Wiley-VCH Verlag GmbH & Co. KGaA, Weinheim

tostatin,[20] and has applications in the diagnosis and treatment of gastrointestinal disorders including endocrine tumors.[21]

The work outlined in here focuses on the synthesis of (carboxymethyl–dextran)-modified magnetic NPs and its OC conjugate, their use as a T_2 MRI contrast agent and their use as drug carriers. In addition, the effects of the OC-NPs conjugate on pancreatic cancer cells Bx-PC3 and colon cancer cells HCT-116were investigated.

Results and Discussion

Scheme 1. shows after the synthesis of carboxymethyl-dextran (CMD) from dextran in the presence of base and bromoacetic acid, then reacted with freshly prepared Fe_3O_4 magnetic nanoparticles, obtained by precipitation under basic conditions.

As shown in Scheme 1, the freshly prepared Fe_3O_4 magnetic nanoparticles (MNPs) were then coated with CMD, followed by the chemical attachment of octreotide to the-modified NPs, which can be stored freeze-dried.

As a first step in our investigation of this system, we evaluated the content of MNPs in CMD-MNPs and octreotide-conjugated MNPs by spectrophotometry methods using published methologies in order to evaluate the approximate stoichiometries of the systems.[22] The approach is based on the detection of a colored Fe^{II}-1,10-phenanthroline complex with a λ_{max} = 512 nm in the presence of hydroxylamine hydrochloride to avoid oxidation of the Fe^{II} to Fe^{III}.

As shown in Figure S2 (see Supporting Information), the absorbance of the complex is proportional to the Fe^{II} concentration in the range 0.5 mg/L to 10.0 mg/L. According to the standard curve, the content of Fe_3O_4 in CMD-MNPs and CMD-MNPs-OC are calculated as 78.4 and 65.2%, respectively.

Figure S3 compares the FT-IR spectrum of pure CMD (spectrum a) to that of CMD shell on the MNP core (spectrum b). The two new peaks at 542 and 460 cm^{-1} are characteristic of the Fe–O bonds. Furthermore, most of the peaks in spectrum b are red-shifted when compared to the spectrum of pure CMD. For example, the 1741 cm^{-1} (symmetric stretching of C=O bond) peak in spectrum a is shifted to 1595 cm^{-1} in spectrum b. The red-shifts are indicative of the coordination of carboxy and hydroxy groups of the CMD molecules with the Fe^{2+} and Fe^{3+} centers. At neutral pH, it has been reported that both CMD and MNPs are negatively charged. In fact, our zeta potential measurements of the naked MNPs and the CMD-MNPs are consistent with previous findings.[23] Thus, the attachment of CMD onto the MNPs core cannot be attributed to electrostatic interaction. Rather, it is the coordination of the iron centers with the functional groups on CMD that facilitates the formation of the core-shell structure.

As a next step in our investigations, we evaluated the average size of the MPNs by transmission electron microscopy (TEM) and atomic force microscopy (AFM). Figure 1 shows the TEM photograph of MNPs, of CMD-MNPs nanoparticles. TEM reveals that the particles are significantly agglomerated without CMD encapsulation (Figure 1, A). With the help of CMD shell, the MNPs become more dispersed (Figure 1, B), though some core-shell structures are still in contact with each other. The CMD-MNPs become highly dispersed upon sonication of the solution for a few minutes (Figure 1, C). These CMD-MNPs, with an average diameter of 50 nm, can also be easily separated and casted into a different solution. Closer examination of the CMD-MNPs shows that the MNP is enclosed by a fluffy shell (Figure 1, D), whose thickness is approximately 10–20 nm. Since a typical dry dextran film situated onto a solid surface has a thickness of ca. 3.0 nm and is considerably hydrated in aqueous solution, the thickness and morphology revealed by the TEM measurements are reasonable and consistent with those from similar studies.[24]

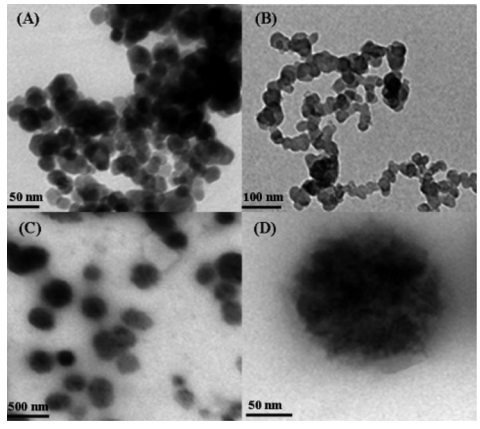

Figure 1. TEM images of (A) MNPs, (B) CMD-MNPs without sonication, (C) CMD-MNPs upon sonication, and (D) a single CMD-MNP.

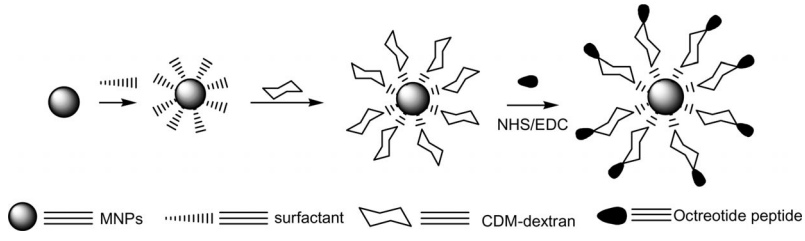

Scheme 1. Stepwise synthesis of octreotide-contjugated magnetic nanoparticles.

 © 2010 Wiley-VCH Verlag GmbH & Co. KGaA, Weinheim

Next, AFM was used to investigate nanoparticles in an aqueous environment. In recent years, compared to ESEM and TEM methods, AFM has become a powerful technique for investigation of NPs, since it allows the study in aqueous environments (contact lense surfaces) and in addition provides information with a spatial resolution relevant to atomic scale measurements.[25]

AFM images for MNPs, and for CMD-MNPs on mica surfaces are shown in Figure 2. It is well known that the surface charge of mica is negative and the ξ-potential of an alginate solution is –71.8 mV.[26] It can be seen that MNPs (Figure 2, A) show compact globe shape. In the presence of CMD, MNPs are regularly dispersed (Figure 2, B), which increase the effective surface area and enhances the amount of octreotide that can be loaded onto the MNPs and potentially will also affect peptide loss from the MNPs.[27]

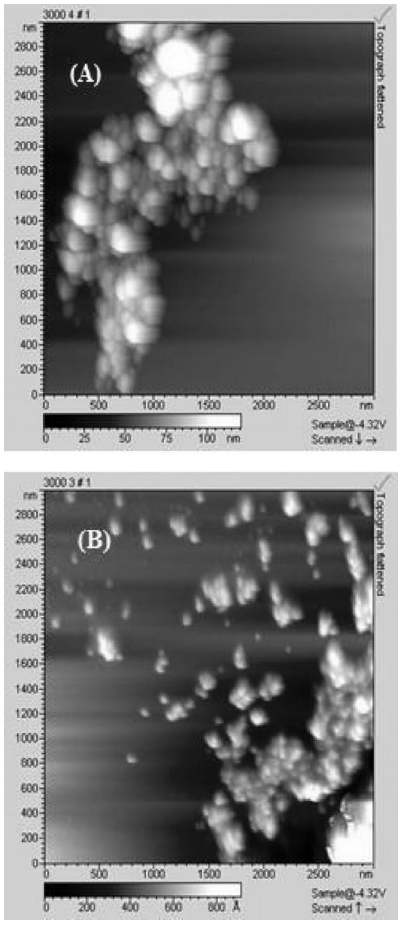

Figure 2. AFM images of (A) MNPs and (B) CMD-MNPs on atomically flat mica surfaces.

As part of our studies, we wanted to evaluate the structure of the Fe_3O_4 and any adverse effects that bioconjugate may have on the MNP core. For this purpose, we carried out powder diffraction study, which enables an evaluation of the crystallinity of the MNP core before and after bioconjugation. Figure S4a shows typical XRD patterns of MNPs. All reflection peaks are assigned to a spinel structure with the characteristic reflections of iron oxide,[28,29] which indicating the presence of a clean crystalline phase the inverse cubic spinel phase of Fe_3O_4.

Figure S4b in the Supporting Information shows the X-ray powder diffraction pattern of CMD-conjugated Fe_3O_4 nanoparticles. As expected, the inverse cubic spinel phase of the MNPs is preserved upon surface modification.

For their ultimate use as targeting agents in MRI applications, it is critical that the iron oxide nanoparticles retain their favourable magnetic properties after being coated with CMD. Figure 3 shows the magnetization curves of our synthesized MNPs before and after coating by CMD as determined by vibrating sample magnetometry (VSM).

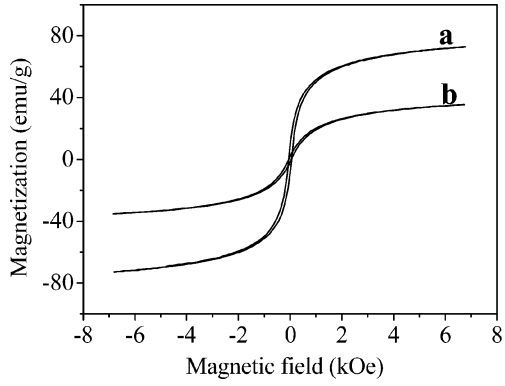

Figure 3. Magnetization curves of nanoparticles (a: MNPs, b: CMD-MNPs).

The saturation magnetization (Ms) of oleic acid-stabilized MNPs was found to be 72 emu g^{-1} at 25 °C, which is better than that reported by Wang and co-workers (60 emu g^{-1}).[30] After coating by CMD, the saturation magnetization decreased to 35 emu g^{-1} as a result of the decrease in Fe_3O_4 content of the nanoparticles (78.4%). This level is acceptable for bio-applications where a saturation magnetization of 7–22 emu g^{-1} is usually required.[31] The nanoparticle size and virtual absence of hysteresis in their magnetic profile suggest that these magnetic nanoparticles are superparamagnetic.[32]

Peptide-related radionuclide therapy (PRRT) is a therapeutic procedure for patients with somatostatin receptor (SSTR) positive tumors in advanced stages.[33] This technique is based on the ability of tumor cells to over-express SSTR, which can be targeted with radio-labeled analogues, which appears to enhance the quality of life in patients.[34] SSTR-positive neuroendocrine tumors (NET) originated in the gastrointestinal tract and the lung in most cases.[35] However, various other non-NET cancers such as sarcomas[36] also show a high level of uptake. Here, we replace the radionuclide by magnetic iron oxide NPs. In view of their water-dispersibility and hollow interior, we tested the capability of the iron oxide MNPs to be used as a T_2 MRI contrast agent. The peptide octreotide (OC), a somatostatin analogue that specifically targets somatostatin receptors, was used as a model drug and drug-delivery vehicle to transport MNPs into biological tissue.[19,37]

 © 2010 Wiley-VCH Verlag GmbH & Co. KGaA, Weinheim

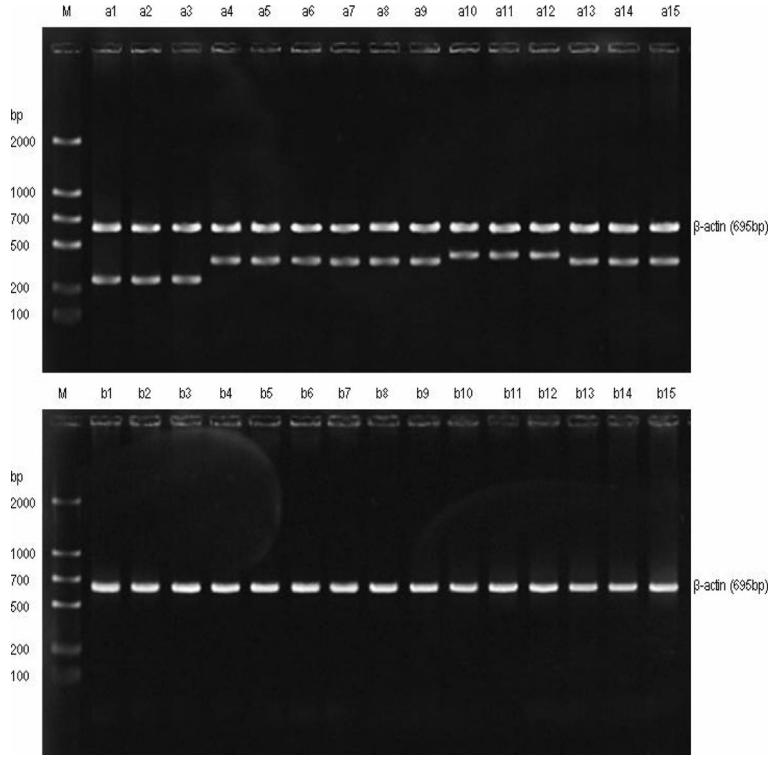

Figure 4. The amplification products of pancreatic cancer cells Bx-PC3 and colon cancer cells HCT-116 somatostatin receptor including five subtypes by RT-PCR; a1-a15: BX-PC3 cell, b1-b15: HCT-116 cell, Lane M: Marker, Lane a1, a2, a3: SSTR1 mRNA expression of BX-PC3 mRNA (303bp), Lane a4, a5, a6: SSTR2 mRNA expression of BX-PC3 mRNA (390bp), Lane a7, a8, a9: SSTR3 mRNA expression of BX-PC3 mRNA (385bp), Lane a10, a11, a12: SSTR4 mRNA expression of BX-PC3 mRNA (433bp), Lane a13, a14, a15: SSTR5 mRNA expression of BX-PC3 mRNA (385bp).

In this project, we choose pancreatic cancer cells Bx-PC3 and colon cancer cells HCT-116 since they differ with respect to a somatostatin receptor and thus their ability to internalize material by endocytosis. Our result of a study employing the reverse transcription polymerase chain reaction (RT-PCR) is shown in Figure 4. Pancreatic cancer cells (BX-PC3 SSTR1–5mRNA and β-actin) show positive expression, but for colon cancer cells (HCT-116) a negative expression is observed except for β-actin. Thus, we decided to use these two cancer cell lines for our further investigations.

Transmission electron microscopy was used to study the internalization of CMD-MNPs-OC into the cancer cells (pancreatic cancer cells Bx-PC3 and colon cancer cells HCT-116). We incubated the two kinds of cancer cells with as-prepared nanoparticles, that is to say, two groups for incubation, Group A: pancreatic cancer cells BxPC-3 and CMD-MNPs-OC; Group B: colon cancer cells HCT-116 and CMD-MNPs-OC. After incubation for 24 h, the TEM images of treated cells were presented in Figure 5.

As shown in Figure 5, Group A, the MNPs (indicated by an arrow) are distributed in the cytoplasm widely without any noticeable aggregation.[20,38,39] For Groups B1 and B2, MNPs appear in lysosomes only. This is due to a lack of endocytosis in the colon cancer cell line, and suggests that uptake of the octreotide-modified MNPs requires somatostatin receptors.

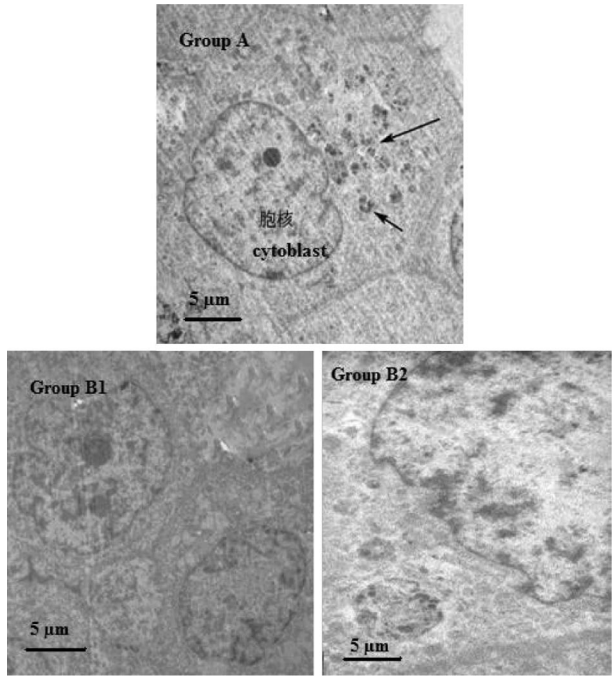

Figure 5. TEM images of two cell lines incubated with OC-CMD-MNPs (Group A: BxPC-3 cell and OC-CMD-MNPs incubate together; Group B1 and Group B2: HCT-116 cell line and OC-CMD-MNPs incubated together).

 © 2010 Wiley-VCH Verlag GmbH & Co. KGaA, Weinheim

For a better understanding of the reaction between our OC-modified MNPs and two cancer cell-lines, and the mechanism of endocytosis, we carried out TEM studies of treated cell after incubation for 24 h, which are stained by HE and Prussian blue. The TEM images are presented in Figures 6 and 7, respectively.

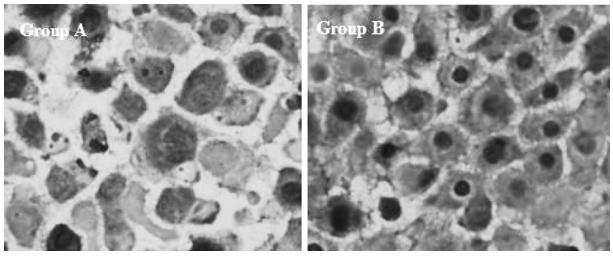

Figure 6. TEM images of HE staining for Group A and Group B. Group A (pancreatic cancer cells BxPC-3 and CMD-MNPs-OC) and Group B (colon cancer cells HCT-116 and CMD-MNPs-OC).

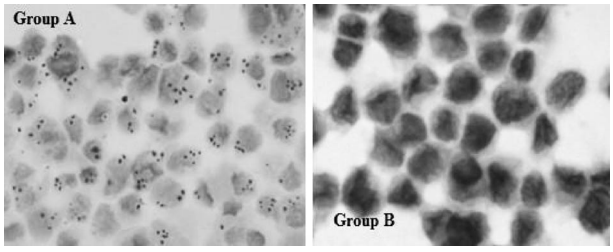

Figure 7. TEM images of Prussian blue staining for Group A and Group B. Group A (pancreatic cancer cells BxPC-3 and CMD-MNPs-OC) and Group B (colon cancer cells HCT-116 and CMD-MNPs-OC).

Figure 6 shows that there is an accumulation of black material in the cytoplasm of the pancreatic cell line BxPC-3 (Group A), suggesting that the MNPs accesses the cytoplasm. The octreotide-conjugated MNPs are recognized by the somatostatin receptor and taken into the cytoplasm. This is in contrast to cells of the colon cancer cell line HCT-116, which do not show the same result due to lack of the somatostatin receptor. In order to confirm our results, we carried out Prussian blue staining which is specific for iron. As Figure 7 shows the presence of MNPs for about 97% of all cells of the pancreatic cancer cell line can be observed, whereas for the colon cancer cell line, the percent of positive cell is only 6% (using a under higher amplification microscope). It is important to point out that these results clearly show the different ability of the two cell lines to interact with our OC-modified MNPs.

Well-dispersed MNPs are important for MRI measurement since effective and controlled MRI contrast can best achieved by evenly distributed functional agents avoiding dead signals that may arise if nanoparticles agglomerate to larger sizes. The use of contrast agents for MRI depends on the ability of the agent to shorten the relaxation times of protons. Positive contrast agents reduce T_1 relaxation times resulting in a brighter signal, while negative contrast agents reduce T_2 resulting in a darker signal.

The reciprocals of the relaxation times are called the relaxation rates, R_1 and R_2, with the effectiveness of a contrast agent expressed as relaxivities, r_1 and r_2, which are determined from the slope of the relaxation rates curve expressed as a function of mM of the total metal concentration.[40] Thus, we carried out MRI experiments on OC-modified MNPs and cancer cells. In order to get very obvious contrast, except for Group A (pancreatic cancer cells BxPC-3 and CMD-MNPs-OC) and Group B (colon cancer cells HCT-116 and CMD-MNPs-OC), we added two more groups, Group C (incubated solution which can be used as black) and Group D (pancreatic cancer cells BxPC-3 and CMD-MNPs) which will has a direct comparison with Group A. The MRI results are shown in Figure 8.

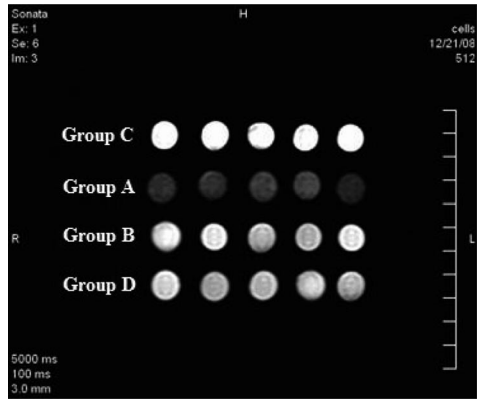

Figure 8. MRI image of four groups, each group having five parallel samples. Group A (pancreatic cancer cells BxPC-3 and CMD-MNPs-OC), Group B (colon cancer cells HCT-116 and CMD-MNPs-OC), Group C (incubated solution which can be used as blank) and Group D (pancreatic cancer cells BxPC-3 and CMD-MNPs).

In Figure 8 shows the results of an MRI study using cell lines in the presence of octreotide-modified MNPs and unmodified MNPs. The strongest signal MRI (white) is observed for the control (Group C, no MNPs added), and the weakest signal (black) is observed for Group A. This suggest that Group A has the highest MNP uptake, consistent with the TEM results. The MNPs presumably access the cytoplasm via endocytosis, and are recognized by the somatostatin receptor. The signal intensity of Group B (non-expression) and D (non-target) are identical and are also higher than for Group A and lower than Group C. This suggests that only very few MNPs are present inside these cells. The signal intensity (SI) value, and the change ratio of signal intensity (ΔSI%) (Group C as control) is presented in Table 1.

Table 1. SI and △SI% of T_2 weighted image for Group A, B and C.

	Group A	Group B	Group C	Group D
SI	382.4 ± 56.4	872.8 ± 36.7	1256.6 ± 31.7	866.6 ± 58.6
ΔSI%	69.6%	30.5%	–	31.0%
	Group A, C and D: $P < 0.001$; Group B and C: $P < 0.001$			

 © 2010 Wiley-VCH Verlag GmbH & Co. KGaA, Weinheim

Group A has the lowest SI value (382.4) in the four groups, consistent with a higher accumulation of MNPs. In addition, the value for ΔSI% (69.6%) is higher than that of B (30.5%) and D (31.0%). Comparing Group A (target) and Group D (non-traget) directly, the ΔSI% decreases from 69.6% to 31.0%.

Conclusions

The synthesis and characterization of a novel conjugate of (carboxymethyl–dextran)-modified magnetic nanoparticles was reported and its activities towards endocytosis into various cell lines and MRI efficacy was tested on pancreatic cancer (Bx-PC3) and colon cancer cell lines (HCT-116) with good results. Interestingly, both cell lines show quite different results. We are currently investigating this in more detail. Overall our work clearly demonstrates the use of octreotide-modified CMD-MNPs for MRI applications. In addition, our results show that OC is an efficient delivery vehicle to transport MNPs to the cytoplasm via endocytosis, and can be used as a MRI probe for SSTR. The future work will focus on using the MRI technology for detecting receptors in an animal model.

Experimental Section

Materials: Dextran T-70 was obtained from Amersham Pharmacia Biotech (Uppsala, Sweden), $FeCl_2$ and $FeCl_3$ were purchased from Futian Chemical Reagent Factory (Tianjin, China). Octreotide was obtained from Novartis Pharma AG (Stein, Switzerland). All other chemicals were analytic grade reagents and used as received without further treatment. Solutions were prepared using deionized water collected from a Millipore Simplicity 185 System (a resistivity of 18.2 MΩcm^{-1} or more, Millipore Co., Billerica, MA).

Syntheses

(1) Synthesis of Carboxymethylation of Dextran: Dextran (2.0 g, 30 μmol) was dissolved in 2 M NaOH (10 mL) containing 0.1 M bromoacetic acid (0.14 g, 1.0 mmol). The solution was stirred for 12 h, dialyzed against water for 24 h, then against 0.1 M HCl for 24 h and finally for 24 h against water. The material is then lyophilized and stored at 4 °C until required for further reactions.

(2) Synthesis of (Carboxymethyl–Dextran)-Modified Magnetic Nanoparticles: Magnetic particles were prepared by the chemical precipitation method. $FeCl_3{\cdot}6H_2O$ (0.5 M, 5.0 mmol) and 0.25 M $FeCl_2{\cdot}4H_2O$ (0.25 g, 2.5 mmol) were dissolved under a N_2 atmosphere in 100 mL of MilliQ water with constant stirring, followed by the addition of the calculated amount of sodium citrate (1.3 g, 5.0 mol). Aqueous ammonia (25–28%, 3.0 g, 50.9 mmol) was dropped into the solution at 65 °C with stirring until pH 9 was reached. The mixture was aged at 80 °C for 30 min. During this time, iron oxide NPs formed. The nanoparticles were collected by filtration under a magnetic field, washed with water to remove unreacted starting materials and any other water-soluble materials. After addition of water and adjusting the pH to 3–4 with diluted hydrochloric acid, the NP suspension was kept at 25 °C for 2 h, followed by the addition of an aqueous solution of CMD (CMD/magnetite weight ratio: 1:3). The suspension was stirred for 6 h at 25 °C and the coated NPs were collected by magnetic separation and washed twice with deionized water to remove excess CMD. Then the wet NPs were freeze-dried and stored until needed at room temperature.

(3) Conjugation of Octreotide to Magnetic Nanoparticles: 10.0 mg of (carboxymethyl–dextran)-modified magnetic nanoparticles were dissolved in 10 mL of Milli Q water and ultrasonicated. Under constant stirring at 25 °C 2 mL of NHS (10 mM) and EDC (10 mM) are added. After activation for 2 h, octreotide (2 μmol, 2.0 mg) was added to the reaction mixture and the suspension was stirred for an additional 6 h at 25 °C. Then the octreotide-MNP were collected by magnetic separation and washed twice with deionized water, followed by freeze-drying of the octreotide-modified nanoparticles.

Characterizations

Determination of Fe^{II} in Magnetic Nanoparticles: The determination of Fe^{II} in the magnetic nanoparticles by spectrophotometry is based on the reaction between 1,10-phenanthroline and Fe^{II}, giving rise to an orange-red colored complex with an absorption maximum at 512 nm. These studies were carried out on a Shimadzu 2450 spectrophotometer (Japan).

Infrared Spectroscopy: Fourier transform infrared (FT-IR) spectra were recorded of samples in the 400–4000 cm^{-1} region in the transmission mode using an Avatar 360 FT-IR spectrometer.

Atomic Force Microscopy: Atomic Force Microscopy (AFM) images were obtained on a PicoScan SPM microscope (Molecular Imaging, Phoenix, AZ) equipped with MAC Mode in which the magnetically coated probe oscillates near its resonant frequency in an alternating magnetic field.

Transmission Electron Microscopy: The size and morphology of nanoparticles were observed by a JEM-1230 transmission electron microscope (Japan).

X-ray Powder Diffraction: The crystal structure was obtained by step scan in an X-ray diffractometer (D/max 2550VB, Japan) with Cu-K_α radiation and a scan range (2θ) of 10–80°.

Magnetic Hysteresis: The magnetic properties of nanoparticles were measured on a HH-15 vibrating sample magnetometer (VSM).

Magnetic Resonance Imaging: All MR Imaging experiments were performed at 1.5 Tesla on a Magnetom Vision machine (Magnetom V16–63, Siemens Medical Systems, Erlangen, Germany), with gradients of 10 mT/m. Data reconstruction was performed by two-dimensional Fourier transformation using a matrix size of 256×256. The samples were placed centrally in a transmit-and-receive coil with an inner diameter of 150 mm and a length of 220 mm. The field of view was 15×15 cm. Measurements were obtained with two acquisitions of a coronally oriented single-slice T_2-weighted multi-spin-echo sequence. Repetition time (TR) was 2000 ms, the echo times (TE) were as follows: 22.5, 45, 67.5, 90, 112.5, 135, 157.5, 180, 202.5, 225, 247.5, 270, 292.5, 315, 337.5, and 360 ms. Measurements of signal intensity on a dedicated workstation (Magic View 3.1, Siemens Medical Systems) were performed directly on the images using an operator-defined region of interest (ROI) with a constant size of 92 pixels. The same ROI positions were measured for all echoes.

Cell Lines

The pancreatic cancer cells Bx-PC3 and colon cancer cells HCT-116 (Xiangya Hospital, Central South University, Hunan, China) over-express somatostatin receptors. The cells were routinely cultivated at 37 °C for 24 h in 50% epoxy resin solution and 50% acetone medium (v:v = 1:1). The treated cells were examined by TEM.

 © 2010 Wiley-VCH Verlag GmbH & Co. KGaA, Weinheim

Supporting Information (see also the footnote on the first page of this article): Information related to the spectroscopic properties (UV/Vis, FT-IR), XRD patterns, zeta-potential measurements, and additional optical microscopy studies.

Acknowledgments

The authors are grateful for financial support of this study by the Natural Science Foundation of China, grant numbers 20676153 and 20876179 (for Y. L.), by the Chinese Ministry of Science and Education (grant numbers 2007AA020810 and 2007AA022006, 863 Program), and by the Hunan Natural Science Foundation (grant 08JJ3043).

[1] L. O. Johansson, A. Bjornerud, H. K. Ahlstrom, D. L. Ladd, D. K. Fujii, *J. Magn. Reson. Imaging* **2001**, *13*, 615–618.
[2] V. R. Ramachandran, I. M. S. Panahi, A. A. Milani, *J. Magn. Reson. Imaging* **2010**, *31*, 46–55.
[3] P. Sun, H. Y. Zhang, C. Liu, J. Fang, M. Wang, J. Chen, J. P. Zhang, C. B. Mao, S. K. Xu, *Langmuir* **2010**, *26*, 1278–1284.
[4] Y. B. Sun, X. B. Ding, Z. H. Zheng, X. Cheng, X. H. Hu, Y. X. Peng, *Macromol. Rapid Comm.* **2007**, *28*, 346–351.
[5] V. M. Bogatyrev, V. M. Gun'ko, M. V. Galaburda, M. V. Borysenko, V. A. Pokrovskiy, O. I. Oranska, E. V. Polshin, O. M. Korduban, R. Leboda, J. Skubiszewska-Zieba, *J. Colloid Interface Sci.* **2009**, *338*, 376–388.
[6] R. B. Zheng, X. W. Meng, F. Q. Tang, *Eur. J. Inorg. Chem.* **2009**, 3003–3007.
[7] B. Xue, Y. Sun, *J. Chromatogr. A* **2002**, *947*, 185–193.
[8] N. Mizutani, T. Iwasaki, S. Watano, T. Yanagida, T. Kawai, *Curr. Appl. Phys.* **2010**, *10*, 801–806.
[9] A. K. Gupta, M. Gupta, *Biomaterials* **2005**, *26*, 3995–4021.
[10] S. Rana, A. Gallo, R. S. Srivastava, R. D. K. Misra, *Acta Biomater.* **2007**, *3*, 233–242.
[11] A. Kaushika, R. Khan, P. R. Solanki, P. Pandey, J. Alam, S. Ahmad, B. D. Malhotra, *Biosens. Bioelectron.* **2008**, *24*, 676–683.
[12] N. Kohler, G. E. Fryxell, M. Q. Zhang, *J. Am. Chem. Soc.* **2004**, *126*, 7206–7211.
[13] Z. F. Xia, G. B. Wang, K. X. Tao, J. X. Li, *J. Magn. Magn. Mater.* **2005**, *293*, 182–186.
[14] K. G. Paul, T. B. Frigo, J. Y. Groman, E. V. Groman, *Bioconjugate Chem.* **2004**, *15*, 394–401.
[15] A. Miyazaki, Y. Tsuda, S. Fukushima, T. Yokoi, T. Vantus, G. Bokonyi, E. Szabo, A. Horvath, G. Keri, Y. Okada, *Bioorg. Med. Chem. Lett.* **2008**, *18*, 6199–6201.
[16] L. Anthony, P. U. Freda, *Curr. Med. Res. Opin.* **2009**, *25*, 2989–2999.
[17] P. Kaczmarek, V. Singh, D. E. Cashen, L. Yang, S. Berk, A. Pasternak, Y. Xiong, D. M. Shen, S. M. Hutchins, K. Chapman, B. Wiedenmann, J. M. Schaeffer, M. Z. Strowski, *Neurogastroenterology and Motility* **2010**, *22*, 204-e66(–203).
[18] S. I. Sersar, A. A. Haneef, A. A. Jamjoom, *J. Cardiac Surgery* **2010**, *25*, 96–96.
[19] A. Giustina, S. Bonadonna, G. Bugari, A. Colao, R. Cozzi, S. Cannavo, L. de Marinis, E. degli Uberti, F. Bogazzi, G. Mazziotti, F. Minuto, M. Montini, E. Ghigo, *Eur. J. Endocrinol.* **2009**, *161*, 331–338.
[20] M. Gabriel, A. Oberauer, G. Dobrozemsky, C. Decristoforo, D. Putzer, D. Kendler, C. Uprimny, P. Kovacs, R. Bale, I. J. Virgolini, *J. Nucl. Med.* **2009**, *50*, 1427–1434.
[21] J. C. Reubi, *Endocr. Rev.* **2003**, *24*, 389–427.
[22] S. M. Chen, C. H. Wang, *Bioelectrochemistry* **2007**, *70*, 452–461.
[23] R. Y. Hong, T. T. Pan, H. Z. Li, *J. Magn. Magn. Mater.* **2006**, *303*, 60–68.
[24] Z. B. Huang, F. Q. Tang, *J. Colloid Interface Sci.* **2004**, *275*, 142–147.
[25] B. Drake, C. B. Prater, A. L. Weisenhorn, S. A. C. Gould, T. R. Albrecht, C. F. Quate, D. S. Cannell, H. G. Hansma, P. K. Hansma, *Science* **1989**, *243*, 1586–1589.
[26] H. L. Ma, X. T. Qi, Y. Maitani, T. Nagai, *Int. J. Pharm.* **2007**, *333*, 177–186.
[27] R. Regmi, C. Black, C. Sudakar, P. H. Keyes, R. Naik, G. Lawes, P. Vaishnava, C. Rablau, D. Kahn, M. Lavoie, V. K. Garg, A. C. Oliveira, *J. Appl. Phys.* **2009**, *106*, 113902-1–113902-9.
[28] X. F. Qu, G. T. Zhou, Q. Z. Yao, S. Q. Fu, *J. Phys. Chem. C* **2010**, *114*, 284–289.
[29] H. Basti, L. Ben Tahar, L. S. Smiri, F. Herbst, M. J. Vaulay, F. Chau, S. Ammar, S. Benderbous, *J. Colloid Interf. Sci.* **2010**, *341*, 248–254.
[30] L. Wang, K. G. Neoh, E. T. Kang, B. Shuter, S. C. Wang, *Adv. Funct. Mater.* **2009**, *19*, 2615–2622.
[31] P. Tartaj, C. J. Serna, *J. Am. Chem. Soc.* **2003**, *125*, 15754–15755.
[32] G. C. Xi, C. Wang, X. Wang, *Eur. J. Inorg. Chem.* **2008**, 425–431.
[33] M. Van Essen, E. P. Krenning, M. De Jong, R. Valkema, D. J. Kwekkeboom, *Acta Oncol.* **2007**, *46*, 723–734.
[34] J. J. M. Teunissen, D. J. Kwekkeboom, E. P. Krenning, P. Krenning, *J. Clin. Oncol.* **2004**, *22*, 2724–2729.
[35] I. M. Modlin, K. D. Lye, M. Kidd, *Cancer* **2003**, *97*, 934–959.
[36] J. W. Friedberg, A. D. Van den Abbeele, K. Kehoe, S. Singer, C. D. Fletcher, G. D. Demetri, *Cancer* **1999**, *86*, 1621–1627.
[37] W. Luboldt, K. Zophel, G. Wunderlich, A. Abramyuk, H. J. Luboldt, J. Kotzerke, *Mol. Imaging Biol.* **2010**, *12*, 78–84.
[38] D. Kozlowska, P. Foran, P. MacMahon, M. J. Shelly, S. Eustace, R. O'Kennedy, *Adv. Drug Delivery Rev.* **2009**, *61*, 1402–1411.
[39] Y. Malam, M. Loizidou, A. M. Seifalian, *Trends Pharmacol. Sci.* **2009**, *30*, 592–599.
[40] D. H. Kim, H. D. Zeng, T. C. Ng, C. S. Brazel, *J. Magn. Magn. Mater.* **2009**, *321*, 3899–3904.

Received: June 30, 2010
Published Online: October 25, 2010

 © 2010 Wiley-VCH Verlag GmbH & Co. KGaA, Weinheim